RSC Advances

PAPER

View Article Online
View Journal | View Issue

Cite this: *RSC Adv.*, 2023, **13**, 13456

Characterization and study of high conductivity antimony-doped tin oxide thin films grown by mist chemical vapor deposition

Li Liu, *[a] Mariko Ueda[b] and Toshiyuki Kawaharamura[abc]

Received 17th January 2023
Accepted 19th April 2023

DOI: 10.1039/d3ra00359k

rsc.li/rsc-advances

Antimony doped tin oxide thin films are grown at atmospheric pressure using a home-built mist chemical vapor deposition system, which is an environmental-friendly technique with low energy consumption. For obtaining high quality Sb:SnO_x films, different solutions are used to support the film fabrication process. The role of each component in supporting solution is also preliminarily analyzed and studied. In this work, the growth rate, density, transmittance, hall effect, conductivity, surface morphology, crystallinity, component and chemical states of Sb:SnO_x films are investigated. Sb:SnO_x films prepared at 400 °C using a mixing solution of H_2O, HNO_3 and HCl show a low electrical resistivity of 6.58 × 10^{-4} Ω cm, high carrier concentration of 3.26 × 10^{21} cm^{-3}, high transmittance of 90%, and wide optical band gas of 4.22 eV. X-ray photoelectron spectroscopy analyses disclose that the samples with good properties have high [Sn^{4+}]/[Sn^{2+}] and [O–Sn^{4+}]/[O–Sn^{2+}] ratios. Moreover, it is discovered that supporting solutions also affect the CBM–VBM level and Fermi level in the band diagram of thin films. These experimental results confirm that Sb:SnO_x films grown using mist CVD are a mixture of SnO_2 and SnO. The sufficient supply of oxygen from supporting solutions leads to the stronger combination of cations and oxygen, and the combination of cations and impurities disappear, which is one of the reasons for obtaining high conductivity Sb:SnO_x films.

Introduction

Tin oxide (SnO_2) thin film is known as a promising material for transparent conducting oxide films (TCOs) because of its outstanding photoelectric properties, high chemical stability and good heat resistance.[1,2] Especially the tin related oxide thin films, such as indium tin oxide (In_2O_3 : SnO_2 = 9 : 1); ITO, fluorine doped tin oxide (SnO_2 : F); FTO, and antimony doped tin oxide (SnO_2 : Sb); ATO, exhibit lower resistivity (10^{-3} to 10^{-4} Ω cm) and higher transmittance (>80%) in the visible region (390–780 nm).[3–5] Among these tin related oxide films, ATO is a candidate doping material with the potential to be studied because the Sb precursor is usually chemically-stable, earth-abundant and non-toxic.[6,7]

However, compared with ITO and FTO films, which have been obtained easily with low resistivity of ~10^{-4} Ω cm, the higher resistivity limits the wide application of ATO films in many fields. According to previous studies, ATO thin films have been prepared using various techniques, such as sputtering,[8] pulsed-laser deposition,[9] metal–organic chemical vapor deposition,[10] aerosol assisted chemical vapor deposition,[11] and spray pyrolysis.[12] With the continuous improvement of fabrication techniques, the ATO films with resistivity in the order of ~10^{-4} Ω cm can be obtained using high growth temperature, highly active precursors, or the subsequent annealing treatment.[10,13]

In this work, ATO thin films were prepared using the 3rd generation mist CVD system, which has a special supply unit including two or more solution chambers and one mixing chamber, and a special reactor with the fine channel (FC) structure. This fine channel type reactor has excellent control over the mist flow for fabricating uniform and high-quality thin films on a large-area substrate under atmospheric pressure. This precious control of mist flow, which makes mist CVD different from spray and AACVD techniques, is achieved by the following physics: the existence of Leidenfrost state droplets (ELSD) and the low probability of collisions between mist droplets (LPCD).[14–18] As reported in some of the literature, the 2nd and 3rd generation mist CVD has been used to fabricate several metal oxide films.[19–23]

Moreover, in contrast to previous research, which improved the film conductivity by optimizing doping ratio and/or increasing growth temperature, we used several liquid materials to support the fabrication process. These liquid materials are called "supporting solution", as they are different from the

[a]*School of System Engineering, Kochi University of Technology, 185 Miyanokuchi, Tosayamada, Kami, Kochi, 782-8502, Japan. E-mail: liu.li@kochi-tech.ac.jp; kawaharamura.toshiyuki@kochi-tech.ac.jp*

[b]*Intelligent Mechr. Sys. Eng. Course, Kochi University of Technology, 185 Miyanokuchi, Tosayamada, Kami, Kochi, 782-8502, Japan*

[c]*Research Institute, Kochi University of Technology, 185 Miyanokuchi, Tosayamada, Kami, Kochi, 782-8502, Japan*

catalysts and react with the precursors in the reactor. In the experiment, ATO thin films were prepared using different supporting solutions. By summarizing and analyzing the experimental results, it was found that the ATO films were mixture of SnO and SnO_2, and the combination of H_2O, HNO_3 and HCl promoted the formation of SnO_2 by increasing the $[Sn^{4+}]/[Sn^{2+}]$ ratio and $[O–Sn^{4+}]/[O–Sn^{2+}]$ ratio, and affected the conductivity, which has never previously been reported.

Experiments

ATO thin films were deposited on quartz under atmospheric pressure by the 3rd generation mist CVD with two solution chambers at 400 °C. Tin(II) chloride dihydrate ($SnCl_2 \cdot 2H_2O$) and antimony(III) chloride ($SbCl_3$) were dissolved in methanol simultaneously (Sb doping ratio was 1.6%) and added to one solution chamber of mist CVD system, while supporting solutions were made with different combinations of H_2O, HNO_3 (69%) and HCl (35.0–37.0%), and were added to the other solution chamber. The detailed growth conditions were shown in Table 1. Quartz substrates were cleaned by sequential sonication in the acetone, isopropanol, and deionized water for 2 min each to remove the surface contamination, and O_3 gas (5000 ppm of O_3 in 1.5 L per min O_2) was used to remove the hydrogen and carbon residues on quartz surface for 2 min at growth temperature. N_2 was chosen as the carrier gas and dilution gas to transport the mist from solution chambers to reactor.

A spectroscopic ellipsometer (J. A. Woollam, W-VASE) was employed to estimate the film thickness (t) and refractive index (n) using the Cauchy model in the transparent region. Sheet resistance (R_s) was studied by a Hall effect setup in the Van der Pauw configuration, the electrical resistivity (R) and conductivity (σ) were determined by the relations: $R = R_s \times t$ and $\sigma = 1/R$. Optical transmittance of sample was measured in the range of 176–2500 nm using UV-Visible spectrometer (Hitachi UV-Vis U-4100). Surface morphology of thin film was measured by Atomic Force Microscope (AFM, Pacific technology Nano-RJ). The crystal structure was analyzed by the X-ray diffraction (XRD) and grazing incident X-ray diffraction (GIXD) using the CuKα radiation (X-ray wavelength $\lambda = 1.5418$ Å, incident angle 0.35°, Rigaku SmartLab). X-ray reflectivity (XRR) was carried out to evaluate the density of thin films. X-ray photoelectron spectroscopy (XPS, AXIS Ultra DLD) was used to investigate the valence states of Sn, the monochromatic Al-Kα ($h\nu = 1486.7$ eV) X-ray source was operated at 40 W and 8 kV at room temperature, and the operating pressure was $<3.0 \times 10^{-8}$ Pa. The binding energies in XPS spectra were calibrated in terms of the peak position of C 1s spectra appearing at 284.8 eV for adventitious carbon surface contamination.[24,25] Ionization energy was measured by photoelectron yield spectroscopy (PYS) (BIP-KV202GD/UVT, Bunkoukeiki Co., Ltd), in which a D2 lamp and photo multiplier were used as a light source and detector, respectively.

Results

In order to precisely study the effects of different supporting solutions on the ATO films, the thicknesses of samples were maintained at approximately 190 nm. However, the differences in film thickness still caused differences in colors. In addition, the different optical properties were also one of the reasons for the difference in film color. Although these four samples showed different colors, they had uniform surfaces without cracks over the whole region area of 30×30 mm^2, as shown in Fig. 1.

Table 2 and Fig. 2 summarized the effects of different supporting solutions on the film deposition rate, refractive index, density and electrical properties. In Fig. 2(a), ATO films prepared with H_2O (sample B) has lower growth rate than the film prepared without supporting. Moreover, sample C and D show lower deposition rates compared to sample B. The film density obtained by XRR measurement is shown in Fig. 2(b). It can be seen that the film density increased from 5.1 g m^{-3} (sample A) to 6.3 g m^{-3} (sample B) by using H_2O support. For

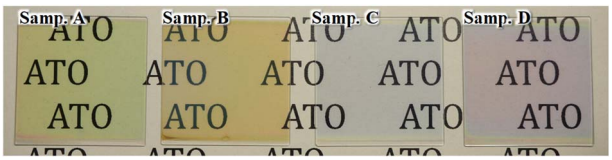

Fig. 1 Photos of ATO films prepared using different supporting solutions.

Table 1 Growth conditions of ATO thin films

		A	B	C	D
Ch. 1[a]	Solute concentration	$SnCl_2 \cdot 2H_2O$, $SbCl_3$ 50 mM, 0.8 mM			
	Solvent	MeOH			
Ch. 2[b]	Supporting solution (composition ratio)	×	H_2O only	H_2O, HNO_3 (99.2 : 0.8)	H_2O, HNO_3, HCl (98.7 : 0.8 : 0.5)
Substrate		30.0 × 30.0 × 0.5 mm^3 Quartz			
c.g/d.g[c] of sol. Ch. 1, L min^{-1}		5.0/0.0			
c.g/d.g of sol. Ch. 2, L min^{-1}		2.0/3.0			
Growth temperature, °C		400			
Growth system		Fine-channel & three-sol.-ch. type mist CVD system			
Ultrasonic transducer		2.4 MHz, 24 V × 0.6 A, 3			

[a] Precursor solution chamber. [b] Supporting solution chamber. [c] Carrier gas/dilution gas.

Table 2 Deposition rate, density, refractive index, resistivity, carrier concentration, and hall mobility values of ATO films prepared with different supporting solutions

	A	B	C	D
Deposition rate (nm min^{-1})	50.9	32.8	19.9	22.7
Density (g cm^{-3})	5.1	6.3	6.7	6.9
Refractive index	2.078	2.002	1.993	1.984
Resistivity (Ω cm)	9.50×10^{-1}	4.85×10^{-3}	6.86×10^{-4}	6.58×10^{-4}
Carrier concentration (cm^3)	3.19×10^{19}	1.79×10^{21}	2.85×10^{21}	3.26×10^{21}
Hall mobility (cm^2 V^{-1} s^{-1})	0.20	0.72	3.20	2.92

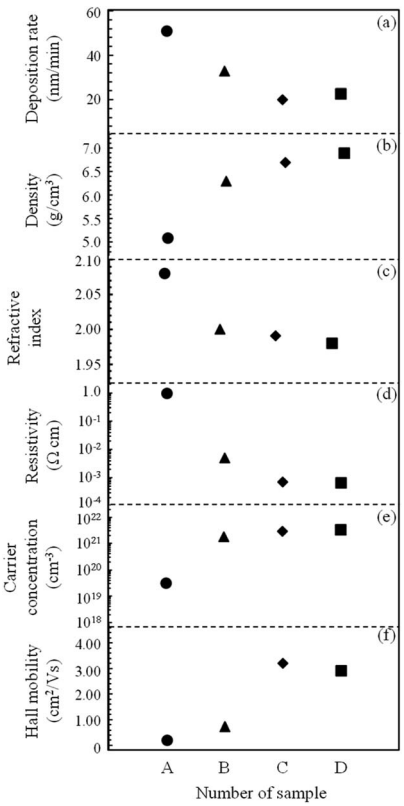

Fig. 2 Summary of (a) deposition rate, (b) density, (c) refractive index and (d), (e), (f) electrical properties of ATO films prepared with different supporting solutions.

sample C and D, HNO_3 and HCl further increased the density to nearly 7.0 g m^{-3}. The decrease in deposition rate and increase in film density are likely due to the use of H_2O as an oxygen source, which reduces the impurities during film formation. Considering that HNO_3 and HCl were used in the preparation of sample C and D, it was deduced that slight acid corrosion from HNO_3 and HCl in supporting solutions affected the deposition rate of films. Fig. 2(c) shows the refractive index of four samples. Typically, the refractive index of pure SnO_2 is 1.90–2.10.[26–28] In this study, the refractive index value (in 550 nm) of sample prepared without support was 2.078, which was larger than that of sample B ($n = 2.002$), C ($n = 1.993$) and D ($n = 1.984$). These results clearly show that the film properties are improved by the supporting solutions.

Fig. 2(d)–(f) summarize the electrical properties of SnO_x:Sb thin films growth using different supporting conditions. In Fig. 2(d), it can be seen that the resistivity significantly decreased from 9.50×10^{-1} Ω cm (sample A) to 4.85×10^{-3} Ω cm (sample B) while using H_2O to support the fabrication. When H_2O + HNO_3 (sample C) and H_2O + HNO_3 + HCl (sample D) were used, the resistivity decreased to 6.84×10^{-4} Ω cm and 6.58×10^{-4} Ω cm respectively, that was dramatically lower than that of sample B. The decrease in resistivity was always accompanied by increasing carrier concentration (n) and Hall mobility (μ), a result consistent with ref. 10, in which it was reported that the film resistivity was associated with the carrier density and Hall mobility. According to previous research, it can be known that Sb may exist in two distinct oxidation states of Sb^{3+} and Sb^{5+} in Sb-doped SnO_2 films.[29–31] When the films prepared without supporting solution, Sb mainly existed in Sb^{3+}. With the use of supporting solutions, Sb^{3+} were oxidized to Sb^{5+}, and the Sb^{5+} replaced on Sn^{4+} sites operated as donor and contributed additional free electrons.[32,33] This substitution phenomenon caused the decrease in film resistivity for sample B–D. Obviously, as one kind of oxygen source, H_2O played an important role in reducing the resistivity. HNO_3 and HCl were absolutely necessary for further reducing the resistivity of ATO films by acting as oxidants in the conversion Sb^{3+} state to Sb^{5+} state. R. L. Rich also concluded that the Sb^{3+} compounds can be oxidized to Sb^{5+} by HNO_3 in previous research.[34]

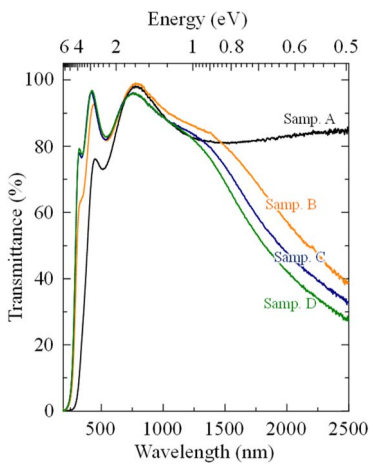

Fig. 3 Optical transmittance spectra of ATO thin films fabricated with different supporting solutions.

In addition to the electrical properties, optical characteristics are also important for high-quality ATO thin films. Fig. 3 shows the optical transmittance spectra of sample A–D prepared on transparent quartz substrates, these spectra in Fig. 3 have deducted that of quartz substrate. The thin films fabricated without supporting solution (sample A) had the lowest average transmittance of ~82% in the visible region (390–780 nm). For samples B, C and D, which were prepared using different supporting conditions, the average transmittances were near 90%. This result illustrates that the supporting solutions are propitious to obtaining the high transparent ATO thin films, while the similar average transmittance of sample B, C and D proves that the effect of H_2O on the transparent is bigger than that of HNO_3 and HCl. In the infrared region (wavelength is greater than 780 nm), the transmittances of sample B, C and D showed a common tendency in that the transmittance decreased with an increase in the wavelength. Considering that the carrier density of sample B, C and D were larger than that of sample A (in Fig. 2(e)), it was determined that the degradation of transmittance in the infrared region was caused by the free-carrier electro-reflection, which also was found in ref. 35. Moreover, the optical band gaps (E_g) of sample A ($E_g = 3.52$ eV), B ($E_g = 4.08$ eV), C ($E_g = 4.20$ eV) and D ($E_g = 4.22$ eV) were also calculated using the relationship $(\alpha h\nu)^2 \propto (h\nu - E_g)$.[36,37] According to previous research, the large E_g values of sample B, C and D were usually caused by the Burstein–Moss effect, which is an apparent effect of the band gap extend caused by the high carrier concentration filling in the orbit.[38,39] In short, the differences in optical band gaps come from the following relationship: $E_g = E_{g0} + \Delta E_{MB}$, where E_{g0} is the intrinsic band gap and ΔE_{MB} is the Burstein–Moss effect.

The surface morphology and crystal structure of samples were confirmed by atomic force microscope and X-ray diffractometer, shown in Fig. 4(a) and (b). In Fig. 4(a), it can be seen that all the ATO films were uniform and without cracks. The sample A, prepared without supporting solution, showed a smooth surface with the root mean square (RMS) roughness of 1.76 nm, which was smaller than that of sample B, C and D. In the images of sample B, C and D, the distribution of obvious grains was continuous and regular on the surface, which reduced the scattering effect, and increased in the transmittance of thin films.

Fig. 4(b) depicts the XRD and GIXD patterns of ATO films. There were small diffraction peaks (110), (101) and (211) appeared in the XRD and GIXD spectra of sample A, indicating that the ATO films prepared by 3rd G mist CVD system had polycrystalline structure. When H_2O was used to support the fabrication process (sample B), the crystallinity was changed. The intensity of peak (110) increased. New preferred peak (200) appeared in the XRD and GIXD spectra, a peak that was also reported in ref. 1, 9, 12 and 40. For sample C and D, the intensity of preferred peak (200) increased and that of peak (110) reduced. Moreover, a slight right shift of peak (200) also appeared in sample C and D. This shift may be caused by the increasing atomic ratio of Sb in the films, which was deduced to be promoted by the HNO_3 in supporting solution.

Components and chemical states of ATO films were confirmed by the Sn $3d_{5/2}$, O 1s and VB edge XPS spectra with Gaussian deconvoluted curves, and shown in Fig. 5(a)–(c). According to the XPS-peak-differentiation-imitating analysis of corresponding Sn $3d_{5/2}$ and O 1s peaks, the atoms of Sn exist at three components corresponding to the Sn^{4+} (BE = 486.8 eV), Sn^{2+} (BE = 486.2 eV) and Sn^0 (BE = 484.8 eV), the O atoms also exist at three components of the O–Sn^{4+} at 530.4 eV, and O–Sn^{2+} at 529.8 eV, O^{Chem} at 531.8 eV, respectively.[41] The existence of different valence states of Sn atoms indicated that the ATO thin films obtained by mist CVD were built-up essentially as a mixture of SnO and SnO_2. In Fig. 5(a) it is clear that the supporting solution increased the $[Sn^{4+}]/[Sn^{2+}]$ ratio. Compared with that of sample B and C, the $[Sn^{4+}]/[Sn^{2+}]$ ratio of sample D which prepared by supporting solution including H_2O, HNO_3 and HCl increased slightly. In Fig. 5(b), H_2O obviously increased the intensity of O–Sn^{4+} component and decreased the intensity of O–Sn^{2+} and O^{Chem} components, proving that H_2O was a strong oxygen source in the fabrication of ATO films. When a mixture of H_2O and HNO_3 was used as supporting solution (sample C), the intensity of O–Sn^{2+} component was further decreased. For sample D, the existence of HCl further reduced the amount of O^{Chem} component. XPS results show that

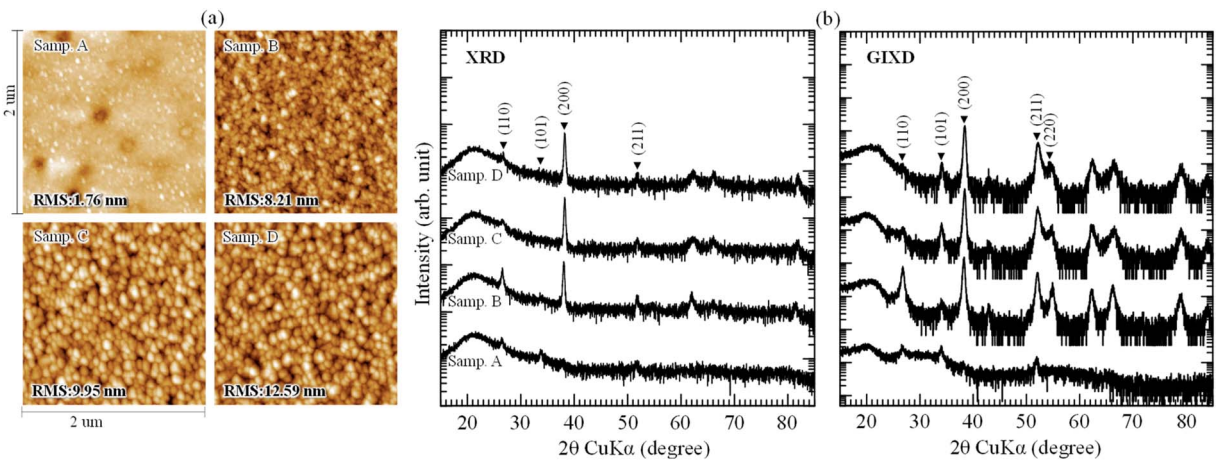

Fig. 4 (a) AFM images and (b) XRD, GIXD spectra of ATO films fabricated with different supporting solutions.

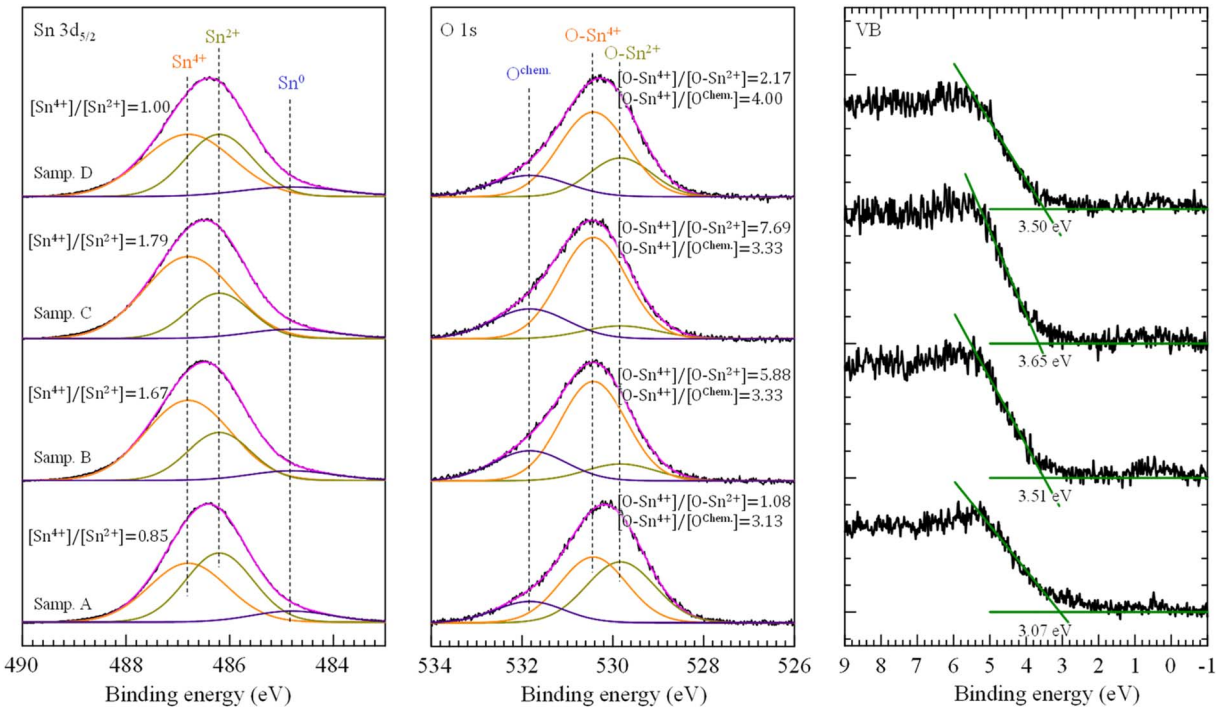

Fig. 5 XPS spectra of Sn $3d_{5/2}$, O 1s and VB obtained from ATO thin films fabricated with different supporting solutions.

the combination of Sn^{4+} and O was improved by the support of H_2O, HNO_3, and HCl + HNO_3, and the improvement tendency may be clarified by the strength of oxidation.

In Fig. 5(c), the values of valence band maximum (VBM) were quantified by extrapolating the leading edge of valence band (VB) spectra to intersect with the background base line. It can be clearly seen that sample B, C, and D show high VBM value, which was attributed to Burstein-Moss effect caused by the large carrier density.[42,43]

Fig. 6(a) shown the PYS results of ATO films obtained using different supporting solutions. The measured ionization energy (IE) of sample A is 7.97 eV, while for sample B, C, and D, that value is 8.10 eV. By summarizing and analyzing the optical band gap, VBM, and PYS results, the band diagram of samples is obtained, as shown in Fig. 6(b). E_{CBM} is the bottom of conduction band, E_{VBM} is the top of valence band. The supporting materials obviously affected the CBM–VBM level and the Fermi level (E_F). The influence of H_2O on the band diagram is stronger

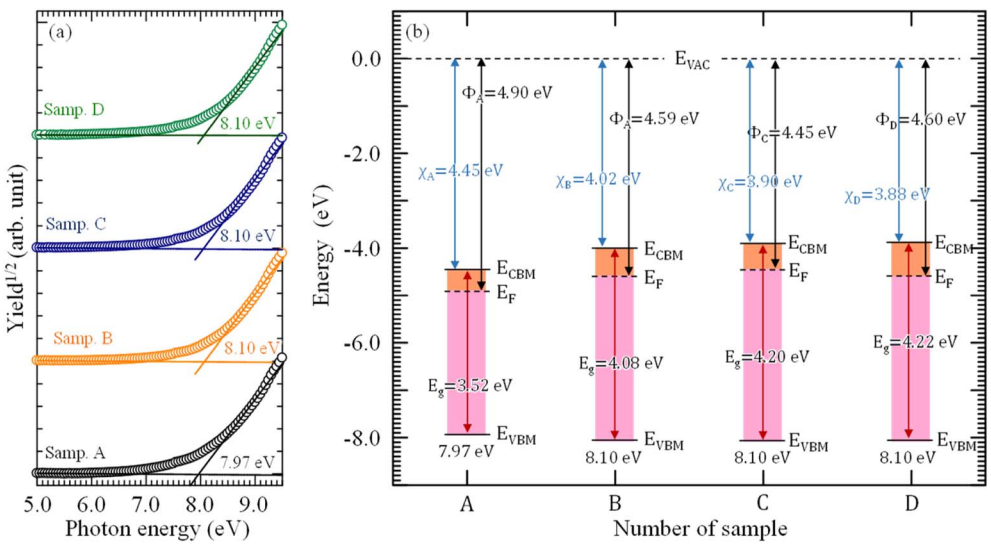

Fig. 6 (a) PYS spectra and (b) energy band diagram of ATO films fabricated with different supporting solutions. Φ is work function, χ is electron affinity, E_g is optical band gap.

than that of HNO_3 or HCl + HNO_3, proving that the H_2O works as an oxygen source, which is important in the fabrication of high quality ATO films. Moreover, similarly to the H_2O, HNO_3 also changes the valence state of Sn, which can be seen from the change of Fermi level of sample C. For HCl, it is more likely to remove the impurities on the sample surface. In the near future, more experiments and studies are necessary to confirm the roles of HCl and HNO_3 in the change of band diagram.

Conclusions

In summary, fabrication of highly conductive thin films with good performances was achieved by 3rd G mist CVD system using different supporting solutions. To study the effects of different supporting materials on the properties of high quality ATO films, the electrical property, optical property, surface morphology, crystal structure, element chemical state in films and band diagram of samples prepared using different supporting solutions were investigated. Experimentally, the following results are obtained:

1. H_2O was an oxygen source, playing an important role in reducing the resistivity; HNO_3 and HCl further reduced the film resistivity, and when mixture solution of H_2O, HNO_3 and HCl were used as supporting solution, the film with low resistivity of 6.58×10^{-4} Ω cm was obtained.

2. The obtained ATO thin films have polycrystalline structure, H_2O promoted the crystallinity of samples and HNO_3 reduced the intensity of peak (110) clearly.

3. These ATO films fabricated by mist CVD system were a mixture of SnO and SnO_2, for the samples prepared without supporting solution, the lack of oxygen source may cause the combination of cations and impurities; when H_2O was used as supporting solution, the sufficient supply of oxygen source lead to the stronger combination of cations and oxygen, and the combination of cations and impurities disappeared.

4. The combination effects of H_2O, HNO_3 and HCl promoted the formation of SnO_2 by increasing the $[Sn^{4+}]/[Sn^{2+}]$ ratio and $[O–Sn^{4+}]/[O–Sn^{2+}]$ ratio, decreasing the content of O^{Chem} components in thin films.

5. The analysis of band diagram illustrates that H_2O can affect the CBM–VBM level and Fermi level; furthermore, HNO_3 works as a strong oxidation and HCl may play a role in cleaning the impurities.

In future experiments, the roles of HCl in fabrication of high quality ATO films will be investigated, and the mechanism by which H_2O, HNO_3 and HCl support the formation of ATO film will also be analyzed and studied.

Conflicts of interest

There are no conflicts to declare.

References

1 T. M. Hammad and N. K. Hejazy, *Int. Nano Lett.*, 2012, **2**, 7–11.
2 T. Minami, S. Takata, H. Sato and H. Sonohara, *J. Vac. Sci. Technol., A*, 1995, **13**, 1095–1099.
3 Y. Ren, Q. H. Wang, X. G. Zhou, Y. Gao and G. Y. Zhao, *J. Electron. Mater.*, 2017, **46**, 6864–6869.
4 Y. Akita, Y. Miyake, H. Nakai, H. Oi, M. Mita, S. Kaneko, M. Mitsuhashi and M. Yoshimoto, *Appl. Phys. Express*, 2011, **4**, 035201.
5 S. H. Yu, L. H. Ding, C. Xue, L. Chen and W. F. Zhang, *J. Non-Cryst. Solids*, 2012, **358**, 3137–3140.
6 F. Chen, J. Y. Wu, Q. Shen, J. M. Schoenung and L. M. Zhang, *Mater. Sci. Forum*, 2014, **783–786**, 1973–1978.
7 J. Montero, J. Herrero and C. Guillén, *Sol. Energy Mater. Sol. Cells*, 2010, **94**, 612–616.
8 H. P. Dang, Q. H. Luc, T. Le and V. H. Le, *J. Nanomater.*, 2016, **2016**, 7825456.
9 S. H. Yu, W. F. Zhang, L. Li, D. Xu, H. L. Dong and Y. X. Jin, *Appl. Surf. Sci.*, 2013, **286**, 417–420.
10 X. J. Feng, J. Ma, F. Yang, F. Ji, F. J. Zong, C. N. Luan and H. L. Ma, *Appl. Surf. Sci.*, 2008, **254**, 6601–6604.
11 S. D. Ponja, B. A. D. Williamson, S. Sathasivam, D. O. Scanlon, I. P. Parkin and C. J. Carmalt, *J. Mater. Chem. C*, 2018, **6**, 7257–7266.
12 A. A. Yadav, *Thin Solid Films*, 2015, **591**, 18–24.
13 M. N. Yusnidar, V. Fauzia, D. Handoko and L. Hanum, *J. Phys.: Conf. Ser.*, 2017, **817**, 012031.
14 T. Kawaharamura, *Jpn. J. Appl. Phys.*, 2014, **53**, 05FF08.
15 P. Rutthongjan, L. Liu, M. Nishi, M. Sakamoto, S. Sato, E. K. C. Pradeep, G. T. Dang and T. Kawaharamura, *Jpn. J. Appl. Phys.*, 2019, **58**, 035503.
16 T. Kawaharamura, G. T. Dang, L. Liu, E. K. C. Pradeep, M. Tatsuta, M. Furuta, Y. Suwa, S. Sato, Y. Nakasone, S. Yamaoki, M. Nishi, Y. Kobayashi, M. Sakamoto, and P. Rutthongjan, *64th JSAP Spring Meeting*, 2017, p. 17a-502-10.
17 T. Kawaharamura, P. Rutthongjan, L. Liu, M. Nishi, M. Sakamoto, Y. Kobayashi, E. K. C. Pradeep, G. T. Dang, S. Sato, S. Yamaoki, Y. Nakasone, and M. Ueda, *78th JSAP Autumn Meeting*, 2017, p. 7a-C17-2.
18 L. Liu, T. Kawaharamura, G. T. Dang, E. K. C. Pradeep, S. Sato, T. Uchida, S. Fujita, T. Hiramatsu, H. Kobayashi and H. Orita, *Jpn. J. Appl. Phys.*, 2019, **58**, 025502.
19 L. Liu, Y. Suwa, S. Sato, Y. Nakasone, M. Nishi, G. T. Dang, E. K. C. Pradeep and T. Kawaharamura, *Jpn. J. Appl. Phys.*, 2017, **56**, 04CJ02.
20 T. Kawaharamura, H. Nishinaka, K. Kametani, Y. Masuda, M. Tanigaki and S. Fujita, *J. Soc. Mater. Sci.*, 2006, **55**, 153–158.
21 T. Igawa, K. Kaneko and S. Fujita, *J. Soc. Mater. Sci.*, 2011, **60**, 994–997.
22 H. J. Jeon, S. G. Lee, H. Kim and J. S. Park, *Appl. Surf. Sci.*, 2014, **301**, 358–362.
23 G. T. Dang, Y. Suwa, M. Sakamoto, L. Liu, P. Rutthongjan, S. Sato, T. Yasuoka, R. Hasegawa and T. Kawaharamura, *Appl. Phys. Express*, 2018, **11**, 111101.
24 T. Uchida, R. Jinno, S. Takemoto, K. Kaneko and S. Fujita, *Jpn. J. Appl. Phys.*, 2018, **57**, 040314.

25 T. Kamimura, K. Sasaki, M. H. Wong, D. Krishnamurth, A. Kuramata, T. Masui, S. Yamakoshi and M. Higashiwaki, *Appl. Phys. Lett.*, 2014, **104**, 192104.
26 D.-w. Choi and J.-S. Park, *Surf. Coat. Technol.*, 2014, **259**, 238–243.
27 J. Heo, S. B. Kim and R. G. Gordon, *Chem. Mater.*, 2012, **22**, 4599–4602.
28 J. W. Elam, D. A. Baker, A. J. Hryn, A. B. F. Martinson, M. J. Pellin and J. T. Hupp, *J. Vac. Sci. Technol. A*, 2008, **26**, 244–252.
29 C. A. Vincent, *J. Electrochem. Soc.*, 1972, **119**, 515–518.
30 E. Elangovan and K. Ramamurthl, *Cryst. Res. Technol.*, 2003, **38**, 779–784.
31 S. Gupta, B. C. Yadav, P. K. Dwivedi and B. Das, *Mater. Res. Bull.*, 2013, **48**, 3315–3322.
32 K. Derrar, M. Zaabat, N. Rouabah, R. Nazir, F. Hanini, A. Hafdallah, S. A. Khan, N. S. Alsaiari, K. Mohammedsaleh Katubi and K. M. Abualnaja, *J. Mater. Sci.: Mater. Electron.*, 2022, **33**, 10142–10153.
33 R. Ramarajan, M. Kovendhan, K. Thangaraju, D. P. Joseph and R. R. Babu, *Appl. Surf. Sci.*, 2019, **487**, 1385–1393.
34 R. L. Rich, *Inorganic Reactions in water*, Springer, Germany, 1st edn, 2008, p. 349.
35 S. Y. Lee and B. O. Park, *Thin Solid Films*, 2006, **510**, 154–158.
36 V. Fauzia, M. N. Yusnidar, L. H. Lalasari, A. Subhan and A. A. Umar, *J. Alloys Compd.*, 2017, **720**, 79–85.
37 B. Stjerna, E. Olsson and C. G. Granqvist, *J. Appl. Phys.*, 1994, **76**, 3797–3817.
38 K. G. Saw, N. M. Aznan, F. K. Yam, S. S. Ng and S. Y. Pung, *PLoS One*, 2015, **10**, e0141180.
39 S. C. Dixon, D. O. Scanlon, C. J. Carmalt and I. P. Parkin, *J. Mater. Chem. C*, 2016, **4**, 6946–6961.
40 M. N. Yusnidar, V. Fauzia, D. Handoko and L. Hanum, *J. Phys.: Conf. Ser.*, 2017, **817**, 012031.
41 J. Szuber, G. Czempik, R. Larciprete, D. Koziej and B. Adamowicz, *Thin Solid Films*, 2001, **391**, 198–203.
42 C. Ke, W. G. Zhu, Z. Zhang, E. S. Tok, B. Ling and J. S. Pan, *Sci. Rep.*, 2015, **5**, 17424.
43 Y. Dou, T. Fishlock, R. G. Egdell, D. S. L. Law and G. Beamson, *Phys. Rev. B*, 1997, **55**, R13381.